nature communications

Article

https://doi.org/10.1038/s41467-024-51997-0

Nickel-catalyzed, silyl-directed, ortho-borylation of arenes via an unusual Ni(II)/Ni(IV) catalytic cycle

Received: 9 February 2024

Accepted: 21 August 2024

Published online: 30 August 2024

Check for updates

Xiaoshi Su[1], Guoao Li[1], Linke He[1], Shengda Chen[1], Xiaoliang Yang[2], Guoqiang Wang[1] ✉ & Shuhua Li[1] ✉

Nickel-catalyzed C−H bond functionalization reactions provide an impressive alternative to those with noble metal catalysts due to their unique reactivity and low cost. However, the regioselective C(sp^2)−H borylation reaction of arenes accomplished by nickel catalyst remains limited. We herein disclose a silyl-directed ortho C(sp^2)−H borylation of substituted arenes with a $Ni(cod)_2$/PMe_3/KHMDS catalyst system. Using readily available starting materials, this protocol provides easy access to ortho-borylated benzylic hydrosilanes bearing flexible substitution patterns. These products can serve as versatile building blocks for the synthesis of sila or sila/borine heterocycles under mild conditions. Control experiments and DFT calculations suggest that a catalytic amount of base prompts the formation of Ni(II)-Bpin-ate complex, likely related to the C(sp^2)−H bond activation. This borylation reaction might follow an unusual Ni(II)/Ni(IV) catalytic cycle.

Organoboron compounds are highly valuable building blocks in the pharmaceutical industry and in the field of organic materials[1]. Catalytic processes that enable the conversion of an inert C−H bond into a C−B bond are currently experiencing tremendous attention because they obviate the need for substrate pre-functionalization[2–7]. Transition-metal-catalyzed C−H bond activation is one of the most powerful strategies[8]. It is typically catalyzed with the most notable examples being the iridium-catalyzed C(sp^2)−H borylation reactions pioneered by the groups of Marder, Hartwig, and Smith[9–12]. Recently, first-row transition metals have been recognized as a sustainable alternative to noble metals due to their unique reactivity, and high earth-abundant resources (including some examples on C−H bond borylation)[5,13–17]. Among others, nickel catalysts have shown great potential for C−H bond functionalization via both directed and non-directed strategies[18,19]. Despite impressive developments of nickel catalysis in cross-coupling reactions[20,21], their application in C−H bond borylation reactions is still an underdeveloped field.

Regioselective borylation of aromatics using nickel catalysis has been limited to activated arenes, such as indoles and pyrroles. Impressive progress has been made by the Chatani[22], Itami[23], Mandal[24], and Marder groups[25] in achieving C2 or C3 selective borylation of indoles (Fig. 1a, top). The regioselectivity of these electron-rich substrates is primarily determined by the intrinsic pK_a values of the corresponding C−H bonds in the case of N-substituted indoles[22], or by traceless directed strategy for N−H indoles[25]. However, when extending these strategies to simple arenes such as substituted benzenes, a mixture of regioisomers (ortho-/meta-/para-, and/or benzylic position) is obtained (Fig. 1a, bottom)[22–24]. Moreover, these reactions require a large excess of arenes due to the low reactivity of the substrates involved. These limitations prompted us to explore nickel-catalyzed regioselective C(sp^2)−H borylation reactions using chelation-assisted C−H bond functionalization strategies. It should be noted that directing groups used in nickel catalysis have been mainly limited to those containing (sp^2)-nitrogen atoms[26]. Therefore, exploring alternative directing groups

[1]Institute of Theoretical and Computational Chemistry, Key Laboratory of Mesoscopic Chemistry of Ministry of Education, School of Chemistry and Chemical Engineering, Nanjing University, Nanjing 210023, P. R. China. [2]State Key Laboratory of Coordination Chemistry, Jiangsu Key Laboratory of Advanced Organic Materials, Chemistry and Biomedicine Innovation Center (ChemBIC), School of Chemistry and Chemical Engineering, Nanjing University, Nanjing 210023, China. ✉e-mail: wangguoqiang710@nju.edu.cn; shuhua@nju.edu.cn

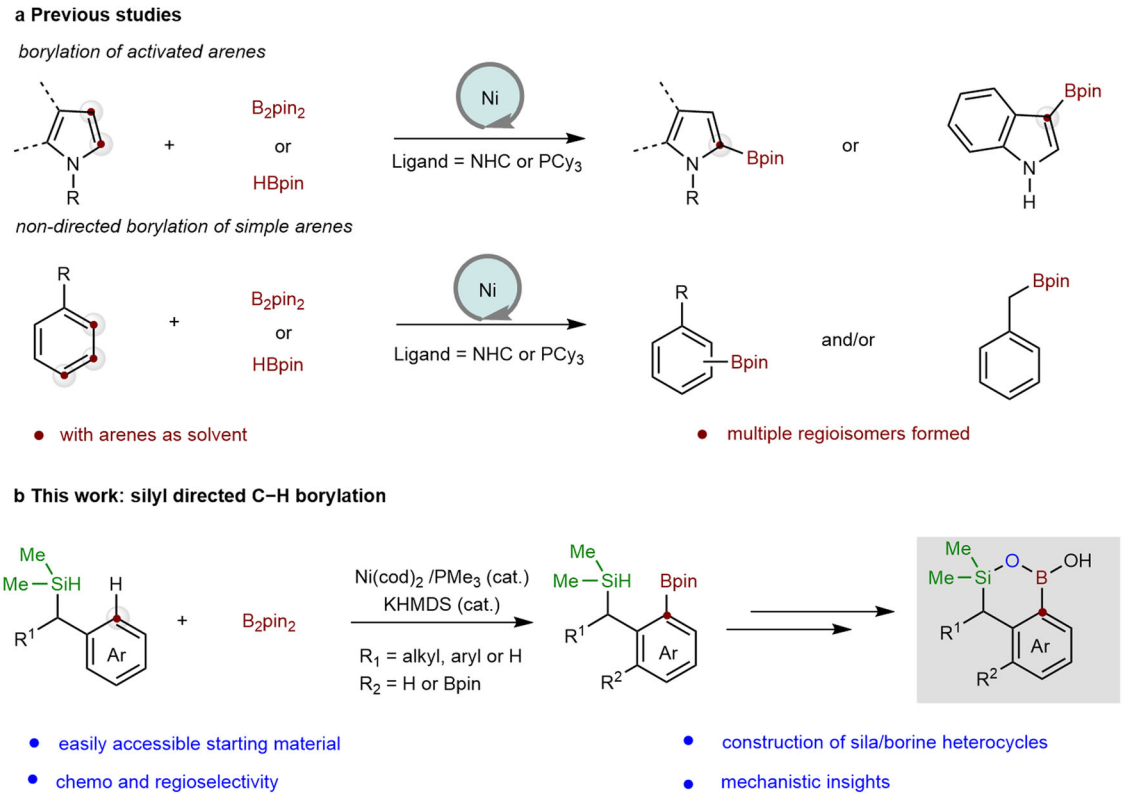

Fig. 1 | Nickel-catalyzed C(sp²)–H borylation reactions. a Current status of nickel-catalyzed C(sp²)–H borylation of arenes. **b** Silyl-directed, ortho-borylation of arenes with nickel catalyst and its application in the construction of sila/borine heterocycles.

for nickel catalysis might lead to more intriguing reactivities. Herein, we report our initial progress in developing the nickel-catalyzed chemo- and regioselective C(sp²)–H borylation reactions of arenes using a modifiable silyl group as the directing group (Fig. 1b). The ortho-borylated product could be readily converted to Si–O–B-containing heterocycles, potentially relevant to medicinal applications. With control experiments and DFT calculations, we propose that a Ni(II)-Bpin-ate complex is the reactive intermediate and an unusual Ni(II)/Ni(IV) catalytic cycle might be responsible for the ortho-selective borylation reaction. This Ni(II)/Ni(IV) catalytic cycle with C–H bond activation mode is very different from previous nickel-catalyzed C(sp²)–H borylation processes that proceed through either a Ni(0)/Ni(II) catalytic cycle or nanoparticle catalysis[22–25].

Results

Reaction discovery and optimization

The silyl group plays a crucial role in synthetic chemistry, particularly as a valuable partner in C–C bond cross-coupling reactions[27,28]. In addition, the carbon–silicon exchange is becoming one of the most important strategies in the area of drug design (Fig. 2a)[29]. Therefore, the direct borylation of organosilicons is highly attractive because the borylated products would provide a wide variety of downstream derivatives via C–Si and/or C–B-based cross-coupling reactions. While silyl-directed C–H borylation reactions have demonstrated effectiveness in iridium catalysis, as shown by Hartwig and colleagues[30–32], several challenges need to be addressed for the realization of the nickel-catalyzed borylation process (Fig. 2b). Firstly, the Si–H bond borylation reaction of hydrosilanes with B_2pin_2 is known to be catalyzed by N-heterocyclic carbene (NHC)-nickel complexes. This suggests that the Si–B coupling pathway (Fig. 2b, **A**) may compete with the C–H borylation process (**B**)[33]. Secondly, unlike the aforementioned processes involving a Ni(0)/Ni(II) catalytic cycle, it remains uncertain whether the corresponding nickel species, after the oxidative addition of the Si–H bond at the nickel center (**C**)[34,35], can further activate the more inert C–H bonds to form a high-valent nickelacycle intermediate (**D**).

To overcome the challenges mentioned above, a thorough screening of ligands, bases as well as nickel precursors is necessary. Initially, we attempted a $Ni(cod)_2$-catalyzed C(sp²)–H borylation reaction of easily accessible benzyldimethylsilane **1a** using B_2pin_2 **2** (Table 1, and see Supplementary Tables 1–6 for details). After some trials, we found that the utilization of $Ni(cod)_2$ (10 mol%) and PMe_3 (10 mol%), and potassium bis(trimethylsilyl)amide (KHMDS) (20 mol%) provided the best results, affording the borylation products **3a** and **3a'** in 83% combined yield with a mono-/bis- ratio of 71:29 (Table 1, entry 1). The utilization of PMe_3 as the ligand avoids the formation of the Si–H borylation product. This is distinct from recent studies on the nickel-catalyzed Si–H borylation reaction with B_2pin_2 by Ito and co-workers[33], in which 1,3-dicyclohexylimidazol-2-ylidene (ICy) was used as the ligand. Replacing PMe_3 with ICy only affords **3a** and **3a'** in 42% yield (Supplementary Table 1). When using the air-stable 16e Ni(0) complex (such as $Ni(^{4\text{-}CF3}stb)_3$, $Ni(^{4\text{-}tBu}stb)_3$) developed by Cornella et al.[36] as the precatalyst, we found that $Ni(^{4\text{-}CF3}stb)_3$ is an efficient Ni(0) source (Table 1, entry 2), while $Ni(^{4\text{-}tBu}stb)_3$ failed to catalyze the reaction (Table 1, entry 3). The Ni(II) precatalysts, such as $Ni(acac)_2$ and $NiCl_2$, are ineffective (Table 1, entry 4). However, $Ni(OTf)_2$ could be a suitable candidate, producing the related borylation product in moderate yield (Table 1, entry 5). The addition of KHMDS was also essential, and there was hardly any formation of borylation product in the absence of KHMDS (Table 1, entry 6). In addition to KHMDS, both ^{t}BuOK, and KH are suitable bases for this transformation, yielding **3a** and **3a'** in moderate yield (Table 1, entries 7–8). The use of a weaker base KOAc did not promote the reaction at all (Table 1, entry 9). It was found that

https://doi.org/10.1038/s41467-024-51997-0

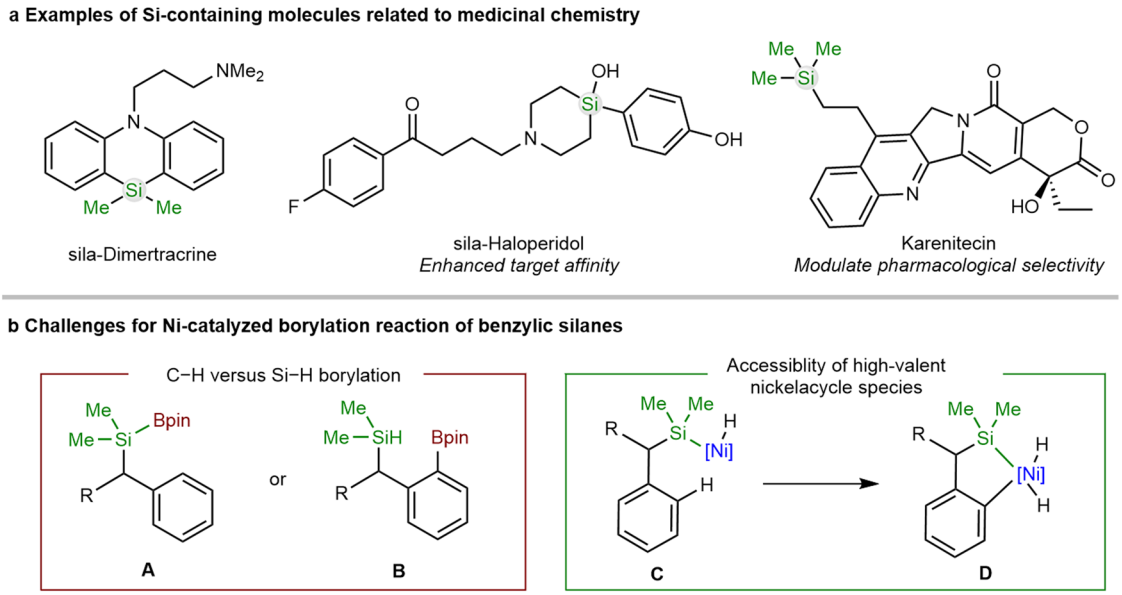

Fig. 2 | Structural importance of Si-containing compounds and potential challenges. a Applications of organosilicons in medicinal chemistry. **b** Synthetic challenges for nickel-catalyzed hydrosilyl-directed C(sp^2)–H borylation reactions.

Table 1 | Optimization of reaction conditions[a]

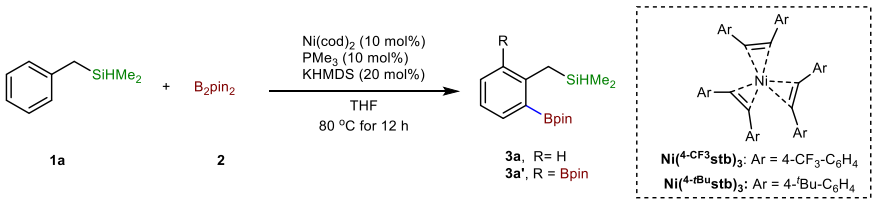

Entry	Variation of standard conditions	3a[b]	3a'[b]
1	None	59%	24%
2	$Ni(^{4\text{-}CF_3}stb)_3$	34%	25%
3	$Ni(^{4\text{-}tBu}stb)_3$	–	–
4	With $Ni(acac)_2$ or $NiCl_2$	–	–
5	$Ni(OTf)_2$ instead of $Ni(cod)_2$	51%	10%
6	Without KHMDS	–	–
7	^{t}BuOK instead of KHMDS	43%	13%
8	KH instead of KHMDS	48%	20%
9	KOAc instead of KHMDS	–	–
10	1.0 equiv. of KHMDS	Trace	69% (52%)[c]
11	Without PMe_3	38%	–
12	PMe_3 (40 mol%)	–	–
13	PCy_3 instead of PMe_3	36%	23%
14	PEt_3 instead of PMe_3	38%	17%
15	PPh_3 or Dcype	–	–
16	At 60 °C	44%	8%
17	At 100 °C	43%	13%

[a]Reaction conditions: **1a** (0.2 mmol), B_2pin_2 (0.6 mmol, 3.0 equiv.), [Ni] (10 mol%), ligand (10 mol%), base (20 mol%) in THF (0.5 mL) at 80 °C for 12 h.
[b]Yields were determined by GC analysis (with $^nC_{18}H_{38}$ as the internal standard).
[c]Isolated yield in 2.5 mmol scales. stb = tris-stilbene.

increasing the amount of KHMDS to 1.0 equivalent results in the formation of bis-borylated product **3a'** in 69% yield along with a trace amount of **3a**, and 52% isolated yield of **3a'** could be obtained in 2.5 mmol scale (Table 1, entry 10). Investigation into the ligand effect shows that in the absence of PMe_3, the yield is greatly reduced (Table 1, entry 11), and the reaction cannot occur normally when the ratio of $Ni(cod)_2$ and PMe_3 is 1:4 (Table 1, entry 12). Other trialkyl phosphines (e.g., PEt_3 and PCy_3) are also effective, although slightly lower yields were observed (Table 1, entries 13–14). No desired product was observed when replacing PMe_3 with PPh_3 or a bidentate

https://doi.org/10.1038/s41467-024-51997-0

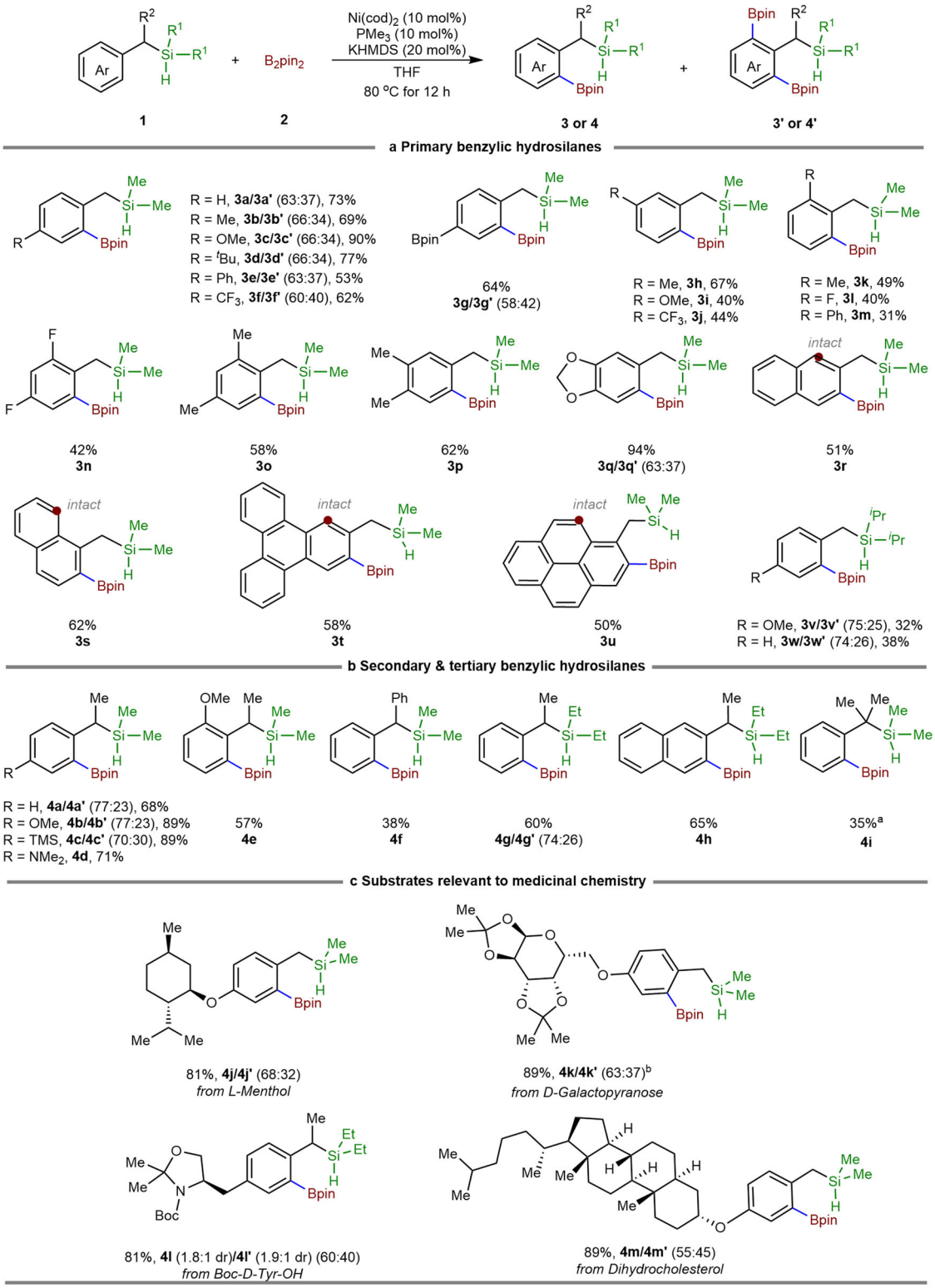

Fig. 3 | Substrate scope. Reaction conditions: benzylic silanes (0.2 mmol), $B_2(pin)_2$ (0.6 mmol), $Ni(cod)_2$ (10 mol%), PMe_3 (10 mol%), KHMDS (20 mmol%), THF (0.5 mL), 12 h, 80 °C. Yields refer to the combined yield of mono- and bis-borylated products, and the ratios were determined after purification. **a** Primary benzylic hydrosilanes. **b** Secondary & tertiary benzylic hydrosilanes. **c** Borylation of substrates relevant to medicinal chemistry. [a]Benzylsilylboronate was obtained in 15% yield. [b]with $Ni(OTf)_2$.

ligand 1,2-bis(dicyclohexylphosphino)ethane (Dcype) (Table 1, entry 15). These results reveal that both the steric and electronic effects of the phosphine ligand are important factors for this silyl-directed borylation process. A diminished yield was observed at lower or elevated temperatures (Table 1, entries 16–17).

Substrate Scope

With the optimal reaction conditions in hand, we explored the substrate scope. As shown in Fig. 3a, electronic and steric effects of the substituent on the aryl ring were investigated with primary benzylic silanes **1b–1g** (para-), **1h–1j** (meta-), **1k–1m** (ortho-). For the prototype reaction,

this ortho-selective borylation process afforded **3a** and **3a'** in 73% combined yield after purification. Both the electron-donating and electron-withdrawing substituents decorated at the para-position of the phenyl ring are well tolerated to deliver the borylated products in moderate to excellent yields (**3b**/**3b'**–**3g**/**3g'**) with mono-/bis- ratios ranging from 58:42 to 66:34, including those with trifluoromethyl (**3f**), and boronate groups (**3g**). The groups of Marder and Martin et al. have demonstrated that C(sp^2)–F or C(sp^2)–O bonds might be converted into the C–B bonds in the presence of a nickel catalyst[37–41]. Here these chemical bonds (**1c**, **1i**, **1l**, etc.) were well compatible with the current conditions. For the substrates with a substituent at the meta-position of the phenyl ring, the regioselectivity is governed by steric hindrance. The borylation reactions occurred at the less hindered positions, producing the corresponding mono-borylated products in moderate to good yields (**3h**–**3j**). Similarly, substrates with ortho-substituents did participate in the borylation reaction, affording the corresponding 1,2,3-trisubstituted arenes in moderate yields (**3k**–**3m**). Tri-substituted substrates were also applicable, providing the corresponding tetrasubstituted arenes in 42–94% yields (**3n**–**3q**). For substrates derived from naphthalenes (**1r** and **1s**), the borylation reactions selectively occurred at the C3 and C2 sites of the naphthalene ring, respectively (**1r** → **3r**, 51% yield; **1s** → **3s**, 62% yield). For the polyaromatic hydrocarbon-type substrates triphenylene and pyrene, the reaction can also undergo smoothly to afford the related monoborylation product (**1t** → **3t**, 58% yield; **1u** → **3u**, 50% yield). It is worth mentioning that the selectivity borylation at the 2-position of pyrenes was also achieved by Marder et al. when employing iridium-based catalysts[42–44]. In comparison with substrates with a dimethyl-silyl directing group (**1a, 1c**), the use of a larger directing group, diisopropyl-silyl (–SiH^iPr_2, **1v** and **1w**), could improve the mono-/bis- ratios, but lower yields were observed.

Substrates with a methyl group at the benzylic position proceed well with improved mono-/bis- ratios (Fig. 3b, **4a**–**d**). With a strong electron donating group at the para position (dimethylamino, **2d**), the reaction only afforded the mono-borylated product **4d** in 71% yield under the standard conditions. Further increasing the steric hindrance of the substrate through the introduction of an –OMe group at the ortho position or a phenyl group at the benzylic position leads to lower borylation efficiency (**4e** and **4f**). Using the –$SiHEt_2$ as the directing group (**2g** → **4g**/**4g'** and **2 h** → **4h**), the borylation reaction outcomes were similar to that with primary derivatives (**1a** → **3a**/**3a'** and **1r** → **3r**). Furthermore, tertiary hydrosilane could also be converted into the mono-borylated product **4i** in 35% yield accompanied by the formation of Si–H bond borylation product in 15% yield.

Furthermore, we examined the synthetic utility of this silyl-directed C–H functionalization reaction in the regioselective functionalization of drug-relevant substrates (Fig. 3c). L-Menthol-derived hydrosilane **2j** successfully underwent the borylation reaction under standard conditions to afford a combined yield of **4j** and **4j'** (81%). D-Galactopyranose derivative **2k** is also tolerated to afford the related borylation products **4k** and **4k'** in 89% yield with $Ni(OTf)_2$ as the catalyst. The reaction of tyrosine derivative **2l** also proceeded well under the standard condition to give mono- and bis-borylation products **4l** and **4l'** in 81% yield. The substrate **2m** derived from hydrocholesterol proceeded with the borylation reaction well to generate the ortho-borylated products **4m**/**4m'** in 89% yields.

Synthetic applications

Figure 4 provides an overview of the practicality of this method and the synthetic applications of the borylation products. In the presence of 2.5 mol% $Ni(cod)_2$, mono-borylated product **3a** and bis-borylated

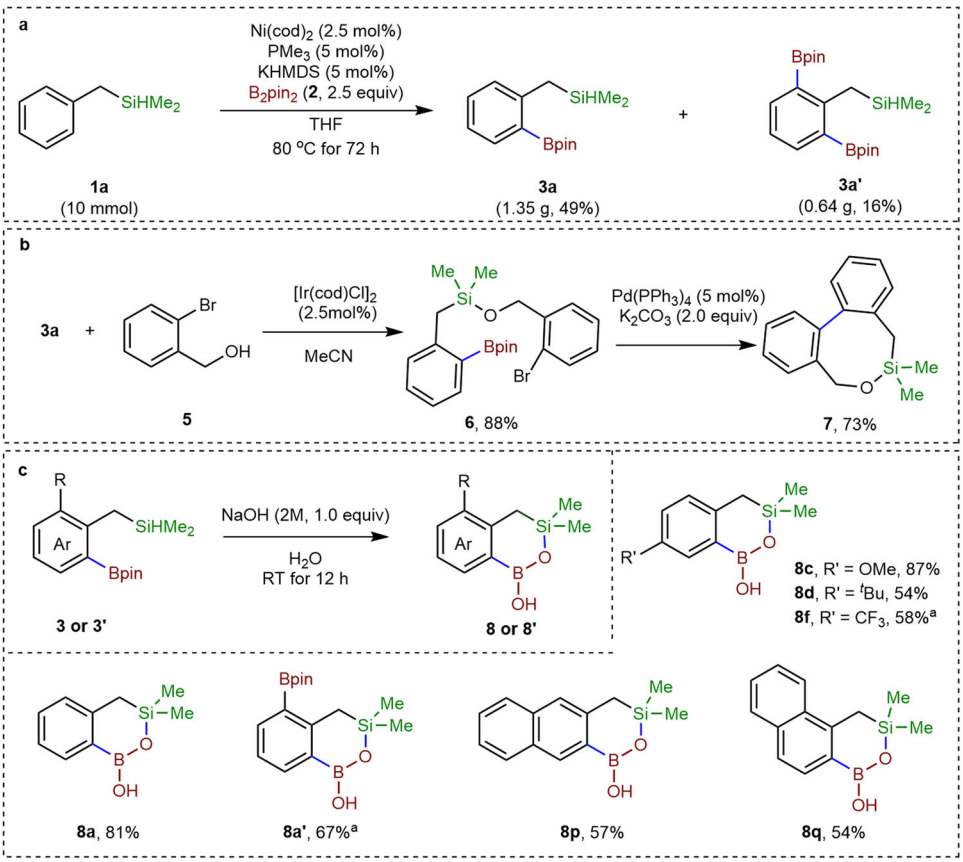

Fig. 4 | Synthetic applications. a Gram-scale synthesis. **b**, **c** Synthetic applications in the construction of Si-containing heterocycles. [a]THF as the reaction solvent.

https://doi.org/10.1038/s41467-024-51997-0

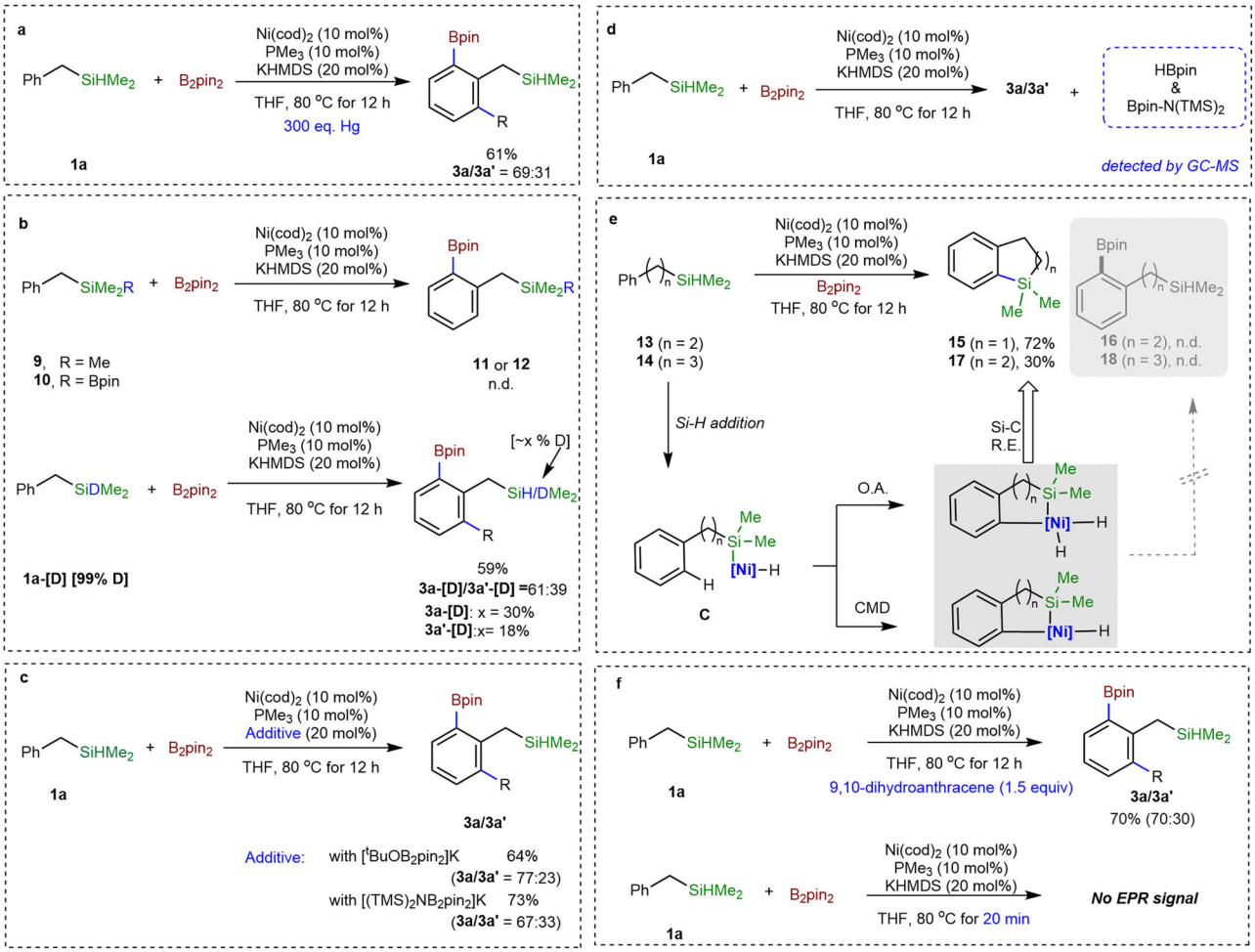

Fig. 5 | Control experiments. a Hg poisoning test. **b** Importance of hydrosilyl group. **c** With Lewis base adduct as the base precursor. **d** Detection of by-products. **e** Involvement of cyclometallic intermediate. **f** Effect of radical scavenger for the standard reaction and EPR experiment on the reaction mixture.

product **3a'** could be prepared in 49% and 16% yields on a 10 mmol scale (Fig. 4a). As both hydrosilanes and boronic esters are easily modifiable groups, the ortho-borylated products could be converted into Si–O–C or Si–O–B–C heterocycles. For example, the Si–H bond and –Bpin in **3a** can be readily converted to an eight-membered heterocycle **7** by applying known methods (Fig. 4b). Upon simply treating the ortho-borylated product with 2 M NaOH aqueous solution, a library of benzo[d][1,2,6] oxasilaborinic heterocycles could be readily constructed (**3** → **8**, Fig. 4c). For the bis-borylation product **3a'**, a similar heterocycle **8a'** could also be obtained leaving the second boryl group untouched. Recently, the carbon–silicon switch strategy has been successfully applied in the agrochemical industry (e.g., flusilazole and silafluofen), and increasing interest has also been drawn in the pharmaceutical industry[45,46]. In addition, boron-containing heterocycles are important in a variety of applications from drug discovery to materials science[47]. This nickel-catalyzed C–H borylation reaction provides economic access to precursors for the construction of Si–O, or Si–O–B containing heterocycles, potentially relevant to medicinal applications.

Mechanistic studies

We then investigated the mechanistic insights into this nickel-catalyzed C(sp^2)–H borylation reaction. Adding an excess amount of mercury did not significantly inhibit the borylation reaction, suggesting that a homogeneous nickel species might be responsible for this silyl-directed borylation process (Fig. 5a)[48]. The experimental outcomes collected in Fig. 5b show that the replacement of the $-SiHR_2$ moiety by $-SiMe_3$ (**9**) or $-SiMe_2Bpin$ (**10**) did not produce the corresponding borylation products (**11/11'** or **12/12'**) under standard conditions. Besides, the reaction of deuterated benzylic hydrosilane **1a-[D]** did proceed well. As determined by ^1H NMR, a certain level of deuterium scrambling was observed in the borylation products (**3a-[D]** and **3a'-[D]**). We noticed that the deuteration rate of **3a'-[D]** was lower than that of **3a-[D]**, suggesting that a C–H/Si–D exchange occurred at the nickel center during the borylation reaction (Fig. 5b). Recently, Marder et al. have thoroughly characterized a series of anionic sp^2-sp^3 diboron adducts[49–51], which might be formed in the current borylation system. Therefore, we analyze the equimolar mixture of KHMDS and B_2pin_2 with $^{11}B\{H\}$ NMR (Supplementary Fig. 16), which exhibited two distinct peaks: one at 31.0 ppm (associated with the sp^2 boron atom) and the other at approximately 3.8 ppm (attributed to the sp^3 tetrahedral boron atom). These results suggest that this base-boron equimolar solution likely contains both B_2pin_2 and the anionic sp^2-sp^3 adduct ($[(TMS)_2NB_2pin_2]^-$). When replacing the base with sp^2-sp^3 diboron complex $[^tBuOB_2pin_2]^-K^+$ or the premixed solution of B_2pin_2 with KHMDS (see Supplementary Figs. 15 and 16), these reactions could also proceed well to afford the related borylation products (Fig. 5c). These results suggest that the Lewis adduct might be a potential intermediate in this borylation reaction. To examine the by-product of the reaction (Fig. 5d), GC-MS analysis of the reaction mixture of borylation of **1a** under standard conditions was conducted, and $(TMS)_2NBpin$ and HBpin were observed (Supplementary Fig. 6), which

https://doi.org/10.1038/s41467-024-51997-0

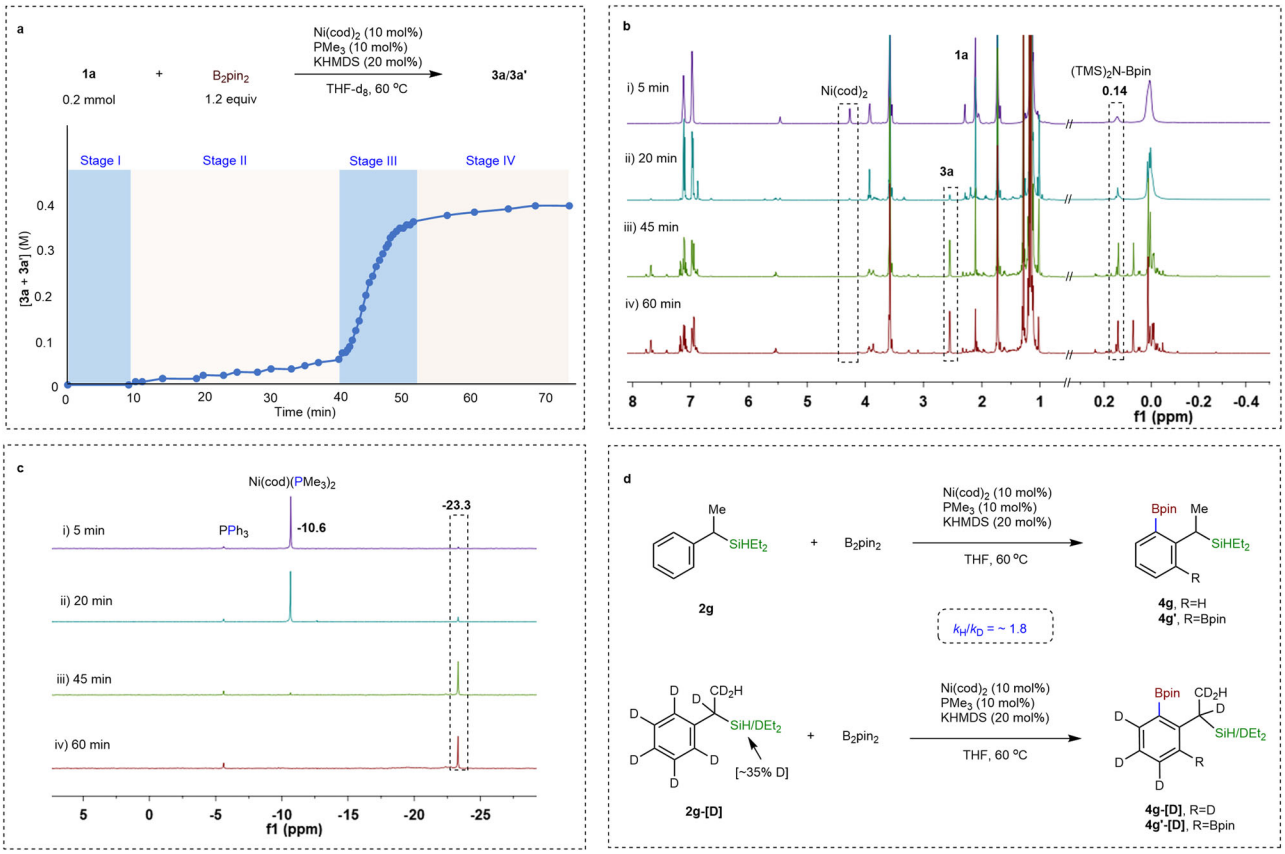

Fig. 6 | Mechanistic experiment. a Plot of the concentration of borylation product (total concentration of **3a** and **3a'**) versus time (min) for the nickel-catalyzed borylation of **1a**. **b** Stacked ^{1}H NMR (600 MHz, THF-d_8) spectra of the reaction. **c** Stacked ^{31}P{H} NMR (162 MHz, THF-d_8) spectra of the reaction (with PPh_3 as an external standard). **d** Parallel kinetic isotopic effects (KIE).

might be associated with the formation of [Ni]−Bpin intermediate. The reaction of phenylethyl silane **13** did not yield the normally borylated product **16** (Fig. 5e). Instead, it resulted in the formation of the intramolecular C−H silylated product benzo[b]silole **15** in 72% yield ($n = 1$). For (3-phenylpropyl)silane **14**, the reaction produced the intramolecular C−H silylated product **17** ($n = 2$). These findings suggest that the oxidative addition of the Si−H bond at the nickel center may take place during the reaction to afford the Ni(II)−silyl species **C** (Fig. 5e)[34,35]. The resulting **C** could then undergo C−H bond activation via oxidative addition or concerted metalation deprotonation (CMD) mechanism, leading to the formation of cyclometallic intermediates. The outcome of the reaction (C−H borylation versus intramolecular C−H silylation) might be influenced by the ring size of the related cyclometallation intermediate. To probe the possibility of a free radical-involved pathway, we examined the reaction in the presence of radical scavenger 9,10-dihydroanthracene (Fig. 5f). No significant influence in the reaction outcome was observed. Besides, electron paramagnetic resonance (EPR) analysis on the standard reaction mixture did not detect any radical signal. These results suggest that the Ni-catalyzed borylation reaction does not involve free radical intermediates or Ni(III) complexes.

Monitoring the C(sp^2)−H borylation reaction of **1a** in THF-d_8 in the presence of B_2pin_2 (1.2 equiv.), $Ni(cod)_2$ (10 mol%) and PMe_3 (10 mol%), and potassium bis(trimethylsilyl)amide (KHMDS) (20 mol%) shows four apparent stages (Fig. 6a)[52]. The first one is the dormant period (Stage I); the second one is the smooth induction period, with only ~10% yield borylation product formed after 30 min (Stage II); the third one is the fastest, the yield of borylation product increased to 58% within 20 min (Stage III); and the fourth one corresponds to the consumption of B_2pin_2 or the possible deactivation of the system (Stage IV).

Based on the kinetic profile, we then collected the ^{1}H NMR spectra from these four stages (Fig. 6b). At the upfield (0.14 ppm), the formation of $(TMS)_2NBpin$ could be detected since Stage I, the signal strength of which rapidly increased during Stage II accompanied by the gradual decrease of KHMDS (at 0.00 ppm). When the reaction entered Stage III, the amount of $(TMS)_2NBpin$ species did not change anymore (about 9% yield, see Supplementary Fig. 10). It has been demonstrated that metal alkoxides (e.g., ^{t}BuOK, KOMe) are suitable bases to promote this nickel-catalyzed borylation reaction (see Supplementary Table 2). Further ^{1}H NMR analysis reveals the explicit formation of the ^{t}BuOBpin (or MeOBpin) species during the reaction when using metal alkoxide as the additive (see Supplementary Fig. 11). These results suggest that the additive KHMDS (or other effective bases) plays a role in inducing the formation of the [Ni]−Bpin intermediate, a possible catalytically reactive species.

The in situ ^{31}P{H} NMR spectra (Fig. 6c, Supplementary Fig. 17) disclose the presence of two peaks, one at −10.6 ppm which is attributed to $Ni(cod)(PMe_3)_2$[53] and another at −23.3 ppm, during both Stage I and II. However, by the time the reaction enters stage III (~45 min), the $Ni(cod)(PMe_3)_2$ is nearly depleted. This observation implies that $Ni(cod)(PMe_3)_2$ is not a resting state or a reactive intermediate in the course of the reaction. The attribution of the principal phosphorus signal at −23.3 ppm in stage III is uncertain, but our further control experiments show that $Ni(PMe_3)_4$ (at about −22.0 ppm) is also inactive for the borylation reaction (see Supplementary Figs. 18 and 19). Thus, we speculate the observed peak at −23.3 ppm might be assigned to a new phosphine-ligated nickel species that potentially catalyzes the borylation reaction. We also conducted parallel kinetic isotope effect (KIE) experiments by measuring the initial rate of the reaction at the steady state (stage III). A relatively obvious KIE (k_H/k_D) of ~1.8 was

https://doi.org/10.1038/s41467-024-51997-0

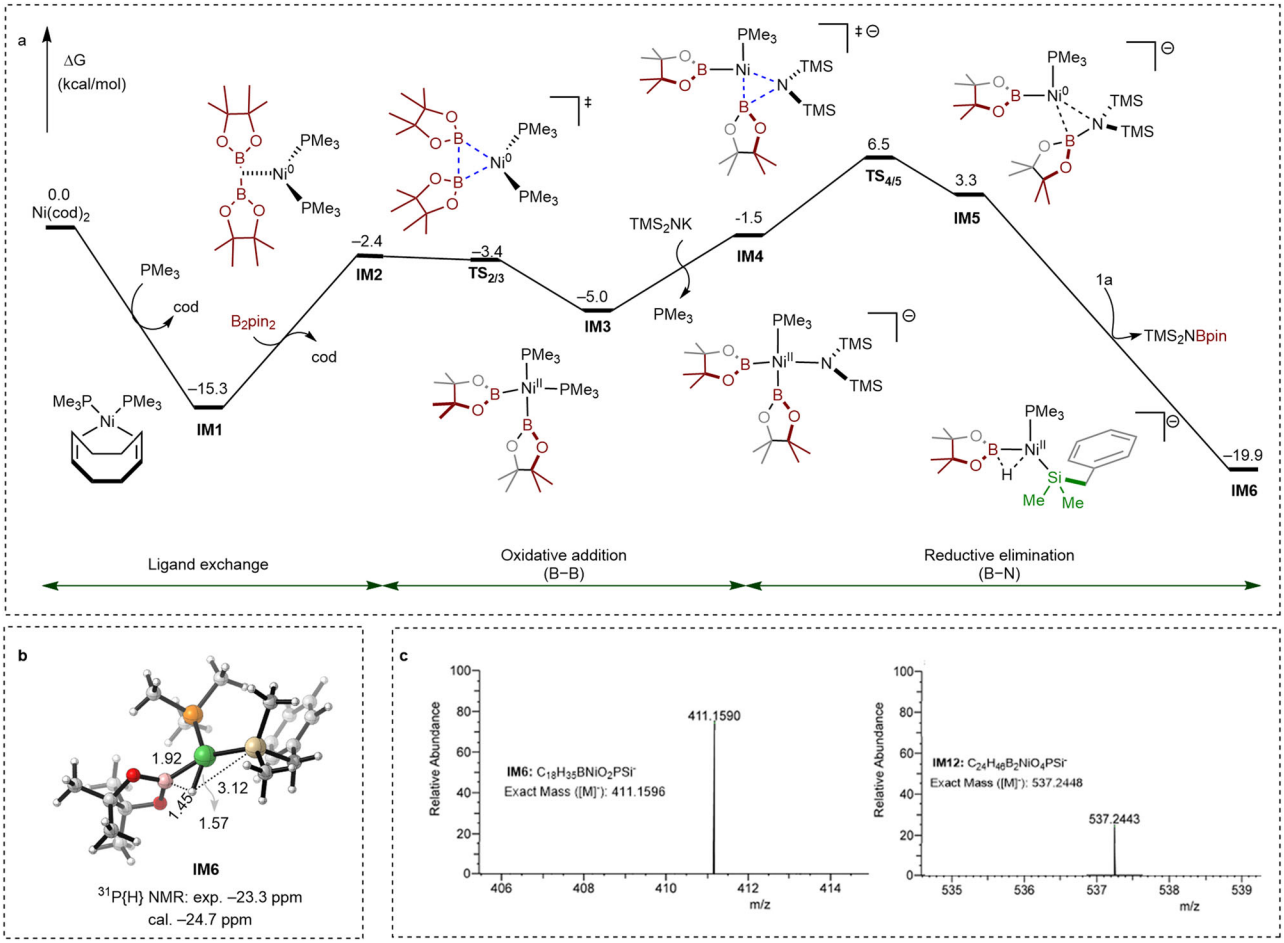

Fig. 7 | DFT calculations. a Calculated free energy profile for the formation of nickelate intermediate **IM6** through the reaction of $Ni(cod)_2$, B_2pin_2, KHMDS, PMe_3 and **1a**. Computed at PCM (THF)/B3LYP-D3/[6-311 + G(d,p) (C, H, O, N, B, Si, P), SDD(Ni)]//B3LYP-D3/[6-31 G(d) (C, H, O, N, B, Si, P), SDD (Ni)] level. **b** The 3D structure and $^{31}P\{H\}$ NMR characterization of the nickelate intermediate **IM6** (Distances are in Å). Color code: H, white; C, gray; B, pink; O, red; P, orange; Si, brown; Ni, green. **c** HRMS characterization of **IM6** and **IM12**.

observed between secondary benzylic silane **2g** and its deuterated form **2g-[D]** (Fig. 6d, see Supplementary Fig. 5 for the reaction outcome of H/D exchange experiment with **2g-[D]** as the substrate). These KIE experiments demonstrate that the C–H activation step is likely the rate-determining step in the catalytic reaction.

DFT calculations

To get more mechanistic insight into this nickel-catalyzed borylation reaction, we also performed DFT calculations with B3LYP-D3 functional using the PCM model to treat the solvent effect[54–58] (basis set details are collected in Supplementary Discussion section). The pathways for the key C–H bond activation were located with the combined molecular dynamics and coordinate driving method (MD/CD)[59]. The borylation reaction between **1a** and B_2pin_2 was chosen as the model reaction. Under the experimental conditions (10 mol% $Ni(cod)_2$ catalyst with 10 mol% PMe_3 and 20 mol% KHMDS, and 3.0 equivalents of B_2pin_2), some different types of Ni(0) complexes might be generated. The energetic details of these species were computed (see Supplementary Fig. 31 for details). Combined control experimentals and DFT computations reveal that $Ni(cod)(PMe_3)_2$ is the most stable nickel Ni(0) complex with exergonic by 15.3 kcal/mol. According to our experimental studies and DFT calculations, the most possible C–H borylation pathway started with the formation of $Ni(cod)(PMe_3)_2$ species **IM1** through the ligand exchange reaction between $Ni(cod)_2$ and PMe_3 (see Supplementary Fig. 42 for the second borylation pathway).

As shown in Fig. 7a, the 18 electron $Ni(cod)(PMe_3)_2$ species **IM1** occurs ligand exchange with B_2pin_2 to form $Ni(B_2pin_2)(PMe_3)_2$ complex **IM2**, which can further undergo an oxidative addition reaction to form a Ni(II)-boryl species **IM3**[60–63]. Then, ligand exchange between **IM3** and KHMDS affords a new Ni(II)-ate complex **IM4**, accompanied by the release of one PMe_3 molecule. Subsequently, **IM4** experiences a reductive elimination of the B–N bond via $\mathbf{TS_{4/5}}$ to generate the intermediate **IM5**. This step carries an activation barrier of 21.8 kcal/mol relative to **IM1**. In **IM5**, the B–N bond coordinates with the nickel center in an η^2-manner. Its further complexation with **1a** generates a Ni complex **IM6**. A comparison with the bond lengths of B–H in free HBpin (1.19 Å) and Si–H in **1a** (1.49 Å) reveals that the B–H and Si–H bonds are cleaved in **IM6** (d_{B-H} = 1.45 Å, and d_{Si-H} = 3.12 Å, Fig. 7b). Therefore, **IM6** might be assigned as a Ni(II) species. The formation of **IM6** is exergonic by 19.9 kcal/mol. It is noteworthy that while **IM1** can undergo successive ligand exchange by reacting with B_2pin_2 and KHMDS, subsequent nickel species (**IM2**-**IM5**) are all less energetically favorable than **IM1**. The computed $^{31}P\{H\}$ NMR chemical shift for **IM6**, which is −24.7 ppm, closely matches the experimentally observed resonance at −23.3 ppm (Fig. 6c). Moreover, the high-resolution mass spectrometry (HRMS) analysis has confirmed the likelihood of the formation of Ni(II)-ate complex **IM6** and its analogous complex **IM12**, related to the second borylation step (Fig. 7c and Supplementary Figs. 23 and 24).

In addition, we also considered other potential pathways related to the formation of **IM6**. These pathways involve the initial Si–H bond

https://doi.org/10.1038/s41467-024-51997-0

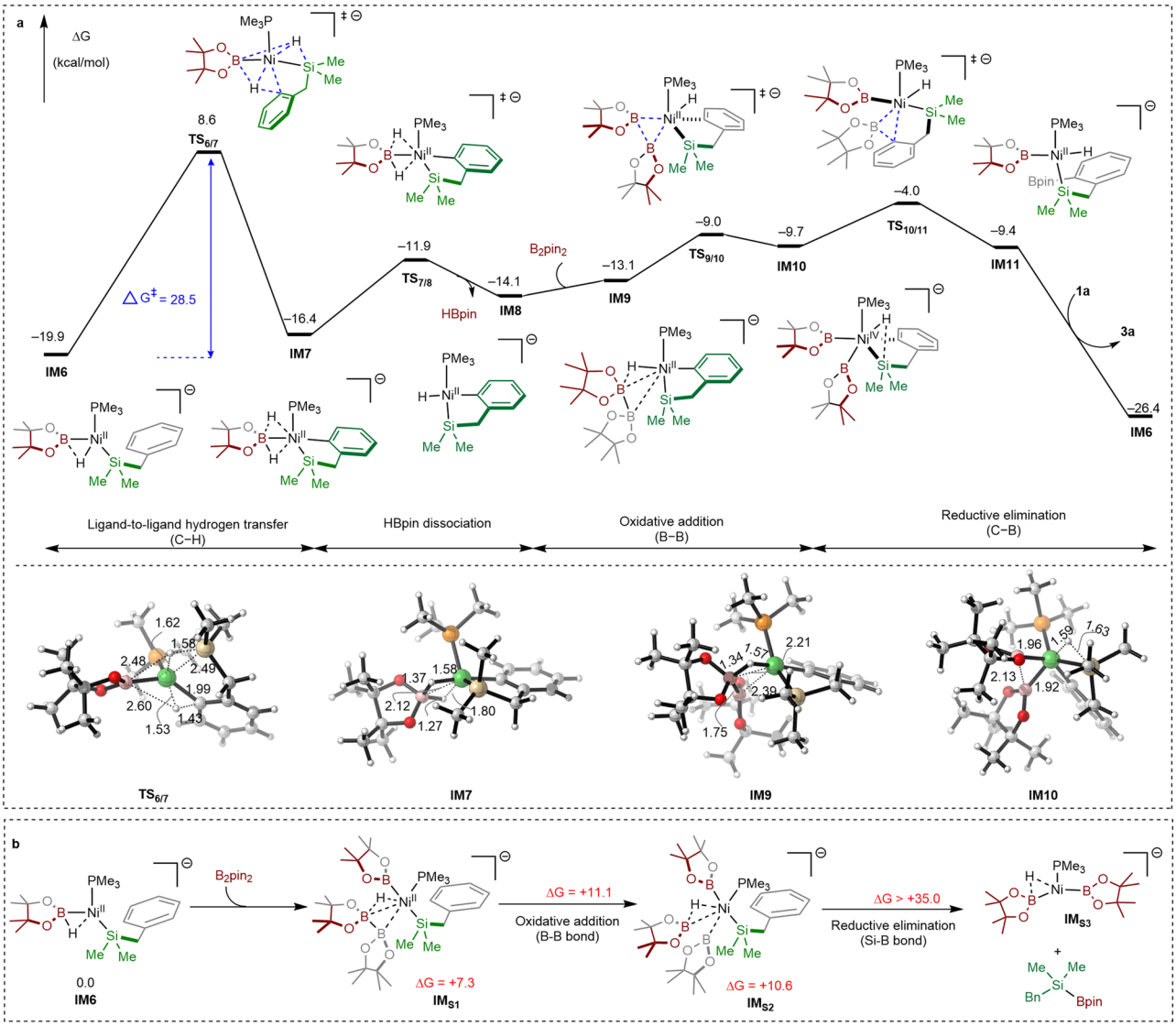

Fig. 8 | DFT Calculations. a Calculated free energy profile and important nickel species for Ni-catalyzed ortho-C−H borylation reaction of benzylic hydrosilane **1a** with nickelate complex **IM6** as the key intermediate. Computed at PCM (THF)/B3LYP-D3/[6-311 + G(d,p) (C, H, O, B, Si, P), SDD(Ni)]//B3LYP-D3/[6-31G(d) (C, H, O, B, Si, P), SDD (Ni)] level. **b** Competing Si−H borylation pathway. Color code: H, white; C, gray; B, pink; O, red; P, orange; Si, brown; Ni, green.

oxidative addition toward $Ni(PMe_3)_2$, followed by the reaction of the diboron compound with the H-Ni(II)-SiR_3 complex or the boryl transfer from the sp^2-sp^3 diboron adduct to the Ni(0) center (see Supplementary Fig. 34 for details). Although the Si−H bond oxidative addition of **1a** with $Ni(PMe_3)_2$ is thermodynamically favorable (ΔG = −8.2 kcal/mol), further boryl group transfer from the $(TMS)_2N$-B_2pin_2 adduct to $\mathbf{IM_{A1}}$ is kinetically unfavorable ($\Delta G^‡$ = 39.0 kcal/mol). Besides, our results indicate that the transfer of the nucleophilic boryl group from the anionic sp^2-sp^3 diboron adduct to the Ni(0) center requires a higher activation barrier compared to the reaction of $Ni(PMe_3)_2$ with the neutral B_2pin_2. This result aligns with our in situ $^{11}B\{H\}$ NMR studies, which revealed no detection of the anionic sp^2-sp^3 diboron adduct during the borylation reaction in the presence of catalytic amounts of KHMDS (see Supplementary Fig. 21). However, when ^{t}BuOK was used as the model base, it was found that both neutral B_2pin_2 and the anionic sp^2-sp^3 diboron adduct can react with the related Ni species with an accessible activation barrier. These results suggest that for the formation of key intermediate **IM6**, different bases might lead to distinct mechanistic pathway. Because the ^{t}BuOK is not the optimal base in this method, the related pathway and discussion are collected in the Supplementary Information (see Supplementary Fig. 36).

Then, **IM6** undergoes a ligand-to-ligand hydrogen transfer[64–66] to form a five-membered cyclometallic nickelate intermediate **IM7** with an activation barrier of 28.5 kcal/mol (Fig. 8a, via $\mathbf{TS_{6/7}}$). In $\mathbf{TS_{6/7}}$, the formation of the Ni−C bond occurs synergistically with a hydrogen transfer from the phenyl ring to the B atom, accompanied by the hydride migration from Ni to the B atom. This C−H activation transition state could be identified through IRC analysis (see Supplementary Fig. 44). **IM7** resembles a nickel-borohydride complex[62], in which two hydrogen atoms are closely bounded to the nickel center. This outcome is consistent with the findings from the deuterium-labeling experiment, which employed a Si−D substrate and demonstrated substantial H/D exchange activity at the $-SiDMe_2$ moiety (cf., Fig. 5b). The two Ni−H and B−H bonds in **IM7** are not equivalent (e.g., $B-H^1$ = 1.37 Å, $Ni-H^1$ = 1.58 Å, and $B-H^2$ = 1.27 Å, $Ni-H^2$ = 1.80 Å). Thus **IM7** has 3 formally anionic ligands and a negative charge and could be assigned to a Ni(II) complex. **IM7** readily dissociates HBpin to generate a Ni(II) intermediate **IM8** (via $\mathbf{TS_{7/8}}$, $\Delta G^‡$ = 4.5 kcal/mol). Subsequently, B_2pin_2 react with **IM8** to generate a Ni(IV) intermediate **IM10** (**IM8** → **IM9** → **IM10**, via $\mathbf{TS_{9/10}}$). In **IM10**, the bond lengths of two Ni−B bonds are 1.92, and 1.96 Å, which are shorter than the sum of the covalent radii of nickel and

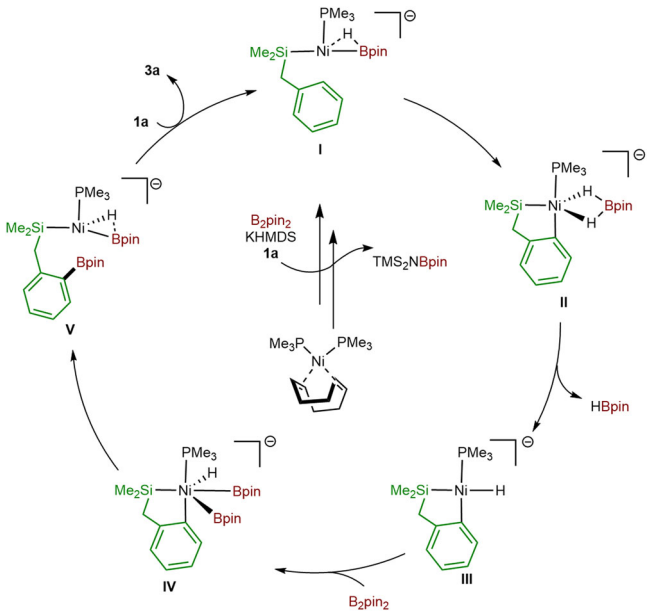

Fig. 9 | Proposed catalytic cycle for nickel-catalyzed silyl-directed C(sp^2)–H borylation reaction. The borylation reaction proceeds through a Ni(II)/Ni(IV) catalytic cycle with Ni(II)-Bpin-ate complex as the key in key intermediate.

boron atoms (2.09 Å). Besides, the B–B distance (2.13 Å) is much longer than that in the free B_2pin_2, indicating a nearly broken B–B bond. The Ni–H distance (1.59 Å) is slightly shorter than the Si–H distance (1.63 Å). Therefore, **IM10** could be assigned to a Ni(IV) species[67,68]. Finally, the reductive elimination of the C–B bond via transition state $\mathbf{TS_{10/11}}$ gives the mono-borylated product **3a** and regenerates the Ni(II)-**1a**-ate complex **IM6**. Along the whole free energy profile, the C–H activation step is the rate-limiting step with a barrier of 28.5 kcal/mol, and this borylation process is exergonic by 26.4 kcal/mol. The barrier for reductive elimination is only 5.7 kcal/mol (with respect to **IM10**), indicating the **IM10** could be considered as a fleeting intermediate. We also studied possible single electron transfer (SET) processes between the Ni(IV) intermediates (**IM10**) and the reducing agents (HBpin, B_2pin_2, and $[(TMS)_2N\text{-}B_2pin_2]^-$) in the reaction system. Our results show that the single electron reduction of Ni(IV) by the boron species are unlikely to happen in the reaction system (Supplementary Table 7). For the rate-determining step, calculations with larger basis sets and other functionals lead to somewhat lower energy barriers (with PWPB95-D4 functional, $\Delta G^{\ddagger} = 20.1$ kcal/mol; with ωB97M-V functional $\Delta G^{\ddagger} = 25.6$ kcal/mol, see Supplementary Table 8). Thus, the calculated free energy profile is qualitatively consistent with the reaction temperature of 80 °C.

It has been shown that the C(sp^2)–H activation via a CMD mechanism is feasible at a Ni(II) center[69]. However, when employing KHMDS as the base, it was found that the C(sp^2)–H activation of Ni(II)-ate complex **IM6** through a classical CMD transition state is thermodynamically unfavorable due to the higher activation barrier required ($\Delta G^{\ddagger} = 53.0$ kcal/mol, see Supplementary Fig. 38 for details). In addition to the C–H borylation pathway, **IM6** could also coordinate with B_2pin_2 to form a Ni(II) intermediate species, $\mathbf{IM_{S1}}$. Then, the oxidative addition of the B–B bond toward the nickel center affords a Ni(IV) intermediate $\mathbf{IM_{S2}}$, which further undergoes a Si–B reductive elimination to generate the Si–H borylation product. Computational results in Fig. 8b revealed that this pathway is unlikely to occur due to the high barrier required for Si–B elimination (see Supplementary Fig. 45 and the related discussions for details). These results can account for the observed selectivity for C–H borylation under experimental conditions.

Proposed catalytic cycle

Based on the control experiments and computational studies, a possible pathway involving a Ni(II)/Ni(IV) cycle might be responsible for this silyl-directed C–H borylation reaction as summarized in Fig. 9. The ortho C–H bond activation step starts with the formation of a [Ni(II)]-(H)(Bpin)(SiR_3) complex **I (IM6)** that might be generated from Ni(cod)(PMe_3)$_2$, KHMDS, B_2pin_2, and **1a** via sequential B–B bond oxidative addition and B–N bond elimination event. Intermediate **I** undergoes a ligand-to-ligand hydrogen transfer event at the Ni(II) center to form a cyclometallation species **II (IM7)**. After the dissociation of HBpin, a cyclometallic Ni(II) intermediate **III (IM8)** is formed. Further, the oxidative addition of B_2pin_2 with concomitant elimination of the C–B bond results in a similar Ni(II)-ate complex **V (IM11)**. Intermediate **V** further undergoes a ligand exchange with **1a**, delivering the final product **3a** and regenerating the reactive catalytic species **I (IM6)**. The detection of Ni(II)-ate complex **I** and two other by-products ($(TMS)_2$NBpin and HBpin) provides strong evidence for the proposed catalytic cycle.

Discussion

In summary, we have described using hydrosilane as a directing group for the ortho-selective borylation of unactivated arenes with B_2pin_2 by employing Ni(cod)$_2$/PMe_3/KHMDS as the catalytic system. This protocol utilizes commercially available catalytic components and provides a facile route to highly substituted arenes that possess two types of modifiable functionalities: hydrosilane and boronate. The resulting ortho-borylated products can serve as versatile dual-functional synthons, as exemplified by the synthesis of sila- or sila/borinine heterocycles, potentially relevant to drug design. DFT calculations combined with experimental studies suggest that a pathway involving an unusual Ni(II)/Ni(IV) catalytic cycle might be responsible for this borylation process.

Methods

General procedure for nickel-catalyzed, silyl-directed, ortho-borylation of arenes

In an argon-filled glovebox, Ni(cod)$_2$ (5.5 mg, 0.02 mmol, 10 mol%), PMe_3 (20 μL, 0.02 mmol, 10 mol%, 1.0 M in THF), KHMDS (40 μL, 0.04 mmol, 20 mol%, 1.0 M in THF), B_2pin_2 (152.4 mg, 0.6 mmol, 3.0 equiv.) and dry THF (0.5 mL) were added to an oven-dried reaction vial. The substrates (0.2 mmol, 1.0 equiv.) were slowly added to the reaction mixture. The reaction vial was capped, removed from the glovebox, and stirred at 80 °C for 12 h. After the reaction was completed, ethyl acetate (10.0 mL) was added to the reaction mixture, then an aliquot (~50 μL) of the reaction solution was subjected to GC-MS and the analysis result indicated the complete consumption of the benzyldimethylsilane. The volatile compounds were removed by rotary evaporation, and the crude product was purified by silica gel column chromatography to afford the pure product.

Data availability

Data related to materials and methods, optimization of conditions, experimental procedures, mechanistic experiments, and spectra are provided in the Supplementary Information. The data supporting the findings of this study are available within this paper and its Supplementary Information. Source data containing the xyz coordinates of the optimized structures. All data are available from the corresponding authors upon request. Source data are provided with this paper.

References

1. Suzuki, A. Cross-coupling reactions of organoboranes: an easy way to construct C–C bonds (Nobel Lecture). *Angew. Chem. Int. Ed.* **50**, 6722–6737 (2011).
2. Mkhalid, I. I. A., Barnard, J. H., Marder, T. B., Murphy, J. M. & Hartwig, J. F. C-H activation for the construction of C-B bonds. *Chem. Rev.* **110**, 890–931 (2010).

3. Ros, A., Fernández, R. & Lassaletta, J. M. Functional group directed C–H borylation. *Chem. Soc. Rev.* **43**, 3229–3243 (2014).
4. Iqbal, S. A., Pahl, J., Yuan, K. & Ingleson, M. J. Intramolecular (directed) electrophilic C–H borylation. *Chem. Soc. Rev.* **49**, 4564–4591 (2020).
5. Bose, S. K. et al. First-row *d*-block element-catalyzed carbon–boron bond formation and related processes. *Chem. Rev.* **121**, 13238–13341 (2021).
6. Tian, Y.-M., Guo, X.-N., Braunschweig, H., Radius, U. & Marder, T. B. Photoinduced borylation for the synthesis of organoboron compounds. *Chem. Rev.* **121**, 3561–3597 (2021).
7. Rej, S. & Chatani, N. Regioselective transition-metal-free C(sp^2)–H borylation: a subject of practical and ongoing interest in synthetic organic chemistry. *Angew. Chem. Int. Ed.* **61**, e202209539 (2022).
8. Bisht, R. et al. Metal-catalysed C–H bond activation and borylation. *Chem. Soc. Rev.* **51**, 5042–5100 (2022).
9. Nguyen, P., Blom, H. P., Westcott, S. A., Taylor, N. J. & Marder, T. B. Synthesis and structures of the first transition-metal tris(boryl) complexes: iridium complexes (.eta.6-arene)Ir($BO_2C_6H_4$)$_3$. *J. Am. Chem. Soc.* **115**, 9329–9330 (1993).
10. Ishiyama, T. et al. Mild iridium-catalyzed borylation of arenes. High turnover numbers, room temperature reactions, and isolation of a potential intermediate. *J. Am. Chem. Soc.* **124**, 390–391 (2002).
11. Cho, J. Y. et al. Remarkably selective iridium catalysts for the elaboration of aromatic C–H bonds. *Science* **295**, 305–308 (2002).
12. Chattopadhyay, B. et al. Ir-catalyzed ortho-borylation of phenols directed by substrate–ligand electrostatic interactions: a combined experimental/in silico strategy for optimizing weak interactions. *J. Am. Chem. Soc.* **139**, 7864–7871 (2017).
13. Su, B., Cao, Z. C. & Shi, Z. J. Exploration of earth-abundant transition metals (Fe, Co, and Ni) as catalysts in unreactive chemical bond activations. *Acc. Chem. Res.* **48**, 886–896 (2015).
14. Dalton, T., Faber, T. & Glorius, F. C– H activation: toward sustainability and applications. *ACS Cent. Sci.* **7**, 245–261 (2021).
15. Roque, J. B. et al. Kinetic and thermodynamic control of C(sp^2)–H activation enables site-selective borylation. *Science* **382**, 1165–1170 (2023).
16. Kamei, T. et al. Ni-catalyzed α-selective C–H borylations of naphthalene-based aromatic compounds. *J. Org. Chem.* **84**, 14354–14359 (2019).
17. Mole, J., Philip, R. M. & Anilkumar, G. Nickel-catalyzed (hetero)aryl borylations: an update. *Arkivok* **part i**, 165–199 (2022).
18. Yamaguchi, J., Muto, K. & Itami, K. Nickel-catalyzed aromatic C–H functionalization. *Top. Curr. Chem.* **374**, 55 (2016).
19. Khake, S. M. & Chatani, N. Nickel-catalyzed C–H functionalization using a non-directed strategy. *Chem* **6**, 1056–1081 (2020).
20. Hazari, N., Melvin, P. & Beromi, M. Well-defined nickel and palladium precatalysts for cross-coupling. *Nat. Rev. Chem.* **1**, 0025 (2017).
21. Guo, L. & Rueping, M. Decarbonylative cross-couplings: nickel-catalyzed functional group interconversion strategies for the construction of complex organic molecules. *Acc. Chem. Res.* **51**, 1185–1195 (2018).
22. Furukawa, T., Tobisu, M. & Chatani, N. Nickel-catalyzed borylation of arenes and indoles via C–H bond cleavage. *Chem. Commun.* **51**, 6508–6511 (2015).
23. Zhang, H., Hagihara, S. & Itami, K. Aromatic C–H borylation by nickel catalysis. *Chem. Lett.* **44**, 779–781 (2015).
24. Das, A., Hota, P. K. & Mandal, S. K. Nickel-catalyzed C(sp^2)–H borylation of arenes. *Organometallics* **38**, 3286–3293 (2019).
25. Tian, Y.-M. et al. Ni-catalyzed trace-less, directed C3-selective C–H borylation of indoles. *J. Am. Chem. Soc.* **142**, 13136–13144 (2020).
26. Khake, S. M. & Chatani, N. Chelation-assisted nickel-catalyzed C–H functionalizations. *Trends Chem.* **1**, 524–539 (2019).
27. Denmark, S. E. & Regens, C. S. Palladium-catalyzed cross-coupling reactions of organosilanols and their salts: practical alternatives to boron- and tin-based methods. *Acc. Chem. Res.* **41**, 1486–1499 (2008).
28. Nakao, Y. & Hiyama, T. Silicon-based cross-coupling reaction: an environmentally benign version. *Chem. Soc. Rev.* **40**, 4893–4901 (2011).
29. Barraza, S. J. & Denmark, S. E. Synthesis, reactivity, functionalization, and ADMET properties of silicon-containing nitrogen heterocycles. *J. Am. Chem. Soc.* **140**, 6668–6684 (2018).
30. Boebel, T. A. & Hartwig, J. F. Silyl-directed, iridium-catalyzed *ortho*-borylation of arenes. A one-pot *ortho*-borylation of phenols, arylamines, and alkylarenes. *J. Am. Chem. Soc.* **130**, 7534–7535 (2008).
31. Robbins, D. W., Boebel, T. A. & Hartwig, J. F. Iridium-catalyzed, silyl-directed borylation of nitrogen-containing heterocycles. *J. Am. Chem. Soc.* **132**, 4068–4069 (2010).
32. Su, B. & Hartwig, J. F. Iridium-catalyzed, silyl-directed, *peri*-borylation of C–H bonds in fused polycyclic arenes and heteroarenes. *Angew. Chem. Int. Ed.* **57**, 10163–10167 (2018).
33. Shishido, R. et al. General synthesis of trialkyl- and dialkylarylsilylboranes: versatile silicon nucleophiles in organic synthesis. *J. Am. Chem. Soc.* **142**, 14125–14133 (2020).
34. Zell, T., Schaub, T., Radacki, K. & Radius, U. Si-H activation of hydrosilanes leading to hydrido silyl and bis(silyl) nickel complexes. *Dalton Trans.* **40**, 1852–1854 (2011).
35. Schmidt, D., Zell, T., Schaub, T. & Radius, U. Si–H activation at $(NHC)_2Ni^0$ leading to hydrido silyl and bis(silyl) complexes: a versatile tool for catalytic Si–H/D exchange, acceptorless dehydrogenative coupling of hydrosilanes, and hydrogenation of disilanes to hydrosilanes. *Dalton Trans.* **43**, 10816–10827 (2014).
36. Nattmann, L., Saeb, R., Nöthling, N. & Cornella, J. An air-stable binary Ni(0)–olefin catalyst. *Nat. Catal.* **3**, 6–13 (2020).
37. Zarate, C., Nakajima, M. & Martin, R. A mild and ligand-free Ni-catalyzed silylation via C–OMe cleavage. *J. Am. Chem. Soc.* **139**, 1191–1197 (2017).
38. Zhou, J. et al. Preparing (multi)fluoroarenes as building blocks for synthesis: nickel-catalyzed borylation of polyfluoroarenes *via* C–F bond cleavage. *J. Am. Chem. Soc.* **138**, 5250–5253 (2016).
39. Tian, Y.-M. et al. Selective photocatalytic C–F borylation of polyfluoroarenes by Rh/Ni dual catalysis providing valuable fluorinated arylboronate esters. *J. Am. Chem. Soc.* **140**, 17612–17623 (2018).
40. Liu, X.-W., Echavarren, J., Zarate, C. & Martin, R. Ni-catalyzed borylation of aryl fluorides via C–F cleavage. *J. Am. Chem. Soc.* **137**, 12470–12473 (2015).
41. Niwa, T., Ochiai, H., Watanabe, Y. & Hosoya, T. Ni/Cu-catalyzed defluoroborylation of fluoroarenes for diverse C–F bond functionalizations. *J. Am. Chem. Soc.* **137**, 14313–14318 (2015).
42. Coventry, D. N. et al. Selective Ir-catalysed borylation of polycyclic aromatic hydrocarbons: structures of naphthalene-2,6-bis(boronate), pyrene-2,7-bis(boronate) and perylene-2,5,8,11-tetra(boronate) esters. *Chem. Commun.* **41**, 2172–2174 (2005).
43. Crawford, A. G. et al. Synthesis of 2- and 2,7-functionalized pyrene derivatives: an application of selective C-H borylation. *Chem. Eur. J.* **18**, 5022–5035 (2012).
44. Ji, L., Lorbach, A., Edkins, R. M. & Marder, T. B. Synthesis and photophysics of a 2,7-disubstituted donor–acceptor pyrene derivative: an example of the application of sequential Ir-catalyzed C–H borylation and substitution chemistry. *J. Org. Chem.* **80**, 5658–5665 (2015).
45. Franz, A. K. & Wilson, S. O. Organosilicon molecules with medicinal applications. *J. Med. Chem.* **56**, 388–405 (2013).
46. Fang, H., Hou, W., Liu, G. & Huang, Z. Ruthenium-catalyzed site-selective intramolecular silylation of primary C–H bonds for synthesis of sila-heterocycles. *J. Am. Chem. Soc.* **139**, 11601–11609 (2017).
47. Das, B. C. et al. Boron-containing heterocycles as promising pharmacological agents. *Bioorg. Med. Chem.* **63**, 116748–116773 (2022).

48. Gärtner, D., Sandl, S. & Wangelin, A. J. Homogeneous vs. heterogeneous: mechanistic insights into iron group metal-catalyzed reductions from poisoning experiments. *Catal. Sci. Technol.* **10**, 3502–3514 (2020).
49. Pietsch, S. et al. Synthesis, structure and reactivity of anionic sp^2-sp^3 diboron compounds: readily accessible boryl nucleophiles. *Chem. Eur. J.* **21**, 7082–7099 (2015).
50. Dewhurst, R. D., Neeve, E. C., Braunschweig, H. & Marder, T. B. sp^2-sp^3 Diboranes: astounding structural variability and mild sources of nucleophilic boron for organic synthesis. *Chem. Commun.* **51**, 9594–9607 (2015).
51. Neeve, E. C., Geier, S. J., Mkhalid, I. A. I., Westcott, S. A. & Marder, T. B. Diboron(4) compounds: from structural curiosity to synthetic workhorse. *Chem. Rev.* **116**, 9091–9161 (2016).
52. Cen, S. & Zhang, Z. The differences between dormant period and induction period in catalytic reactions. *Chemistry* **83**, 369–376 (2020).
53. Despagnet-Ayoub, E., Takase, M. K., Labinger, J. A. & Bercaw, J. E. Reversible 1,2-alkyl migration to carbene and ammonia activation in an N-heterocyclic carbene–zirconium complex. *J. Am. Chem. Soc.* **137**, 10500–10503 (2015).
54. Lee, C., Yang, W. & Parr, R. G. Development of the Colle-Salvetti correlation-energy formula into a functional of the electron density. *Matter Mater. Phys.* **37**, 785–789 (1988).
55. Becke, A. D. Density-functional thermochemistry. III. The role of exact exchange. *J. Chem. Phys.* **98**, 5648–5652 (1993).
56. Grimme, S., Antony, J., Ehrlich, S. & Krieg, H. A consistent and accurate ab initio parametrization of density functional dispersion correction (DFT-D) for the 94 elements H-Pu. *J. Chem. Phys.* **132**, 154104–154122 (2010).
57. Grimme, S., Ehrlich, S. & Goerigk, L. Effect of the damping function in dispersion corrected density functional theory. *J. Comput. Chem.* **32**, 1456–1465 (2011).
58. Tomasi, J. & Persico, M. Molecular interactions in solution: an overview of methods based on continuous distributions of the solvent. *Chem. Rev.* **94**, 2027–2094 (1994).
59. Li, G. et al. Combined molecular dynamics and coordinate driving method for automatically searching complicated reaction pathways. *Phys. Chem. Chem. Phys.* **25**, 23696–23707 (2023).
60. Tendera, L., Kuehn, L., Marder, T. B. & Radius, U. On the reactivity of NHC nickel bis-boryl complexes: reductive elimination and formation of mono-boryl complexes. *Chem. Eur. J.* **28**, e202302310 (2023).
61. Adhikari, D., Huffman, J. C. & Mindiola, D. J. Structural elucidation of a nickel boryl complex. A recyclable borylation Ni(ii) reagent of bromobenzene. *Chem. Commun.* **43**, 4489–4491 (2007).
62. Rios, P. et al. Ambiphilic boryl groups in a neutral Ni(ii) complex: a new activation mode of H_2. *Chem. Sci.* **12**, 2540–2548 (2021).
63. Tendera, L., Fantuzzi, F., Marder, T. B. & Radius, U. Nickel boryl complexes, and nickel-catalyzed alkyne borylation. *Chem. Sci.* **14**, 2215–2228 (2023).
64. Guihaumé, J., Halbert, S., Eisenstein, O. & Perutz, R. N. Hydrofluoroarylation of alkynes with Ni catalysts. C–H activation via ligand-to-ligand hydrogen transfer, an alternative to oxidative addition. *Organometallics* **31**, 1300–1314 (2011).
65. Bair, J. S. et al. Linear-selective hydroarylation of unactivated terminal and internal olefins with trifluoromethyl-substituted arenes. *J. Am. Chem. Soc.* **136**, 13098–13101 (2014).
66. Tang, S., Eisenstein, O., Nakao, Y. & Sakaki, S. Aromatic C–H σ-Bond activation by Ni^0, Pd^0, and Pt^0 alkene complexes: concerted oxidative addition to metal vs ligand-to-ligand H transfer mechanism. *Organometallics* **36**, 2761–2771 (2017).
67. Camasso, N. M. & Sanford, M. S. Design, synthesis, and carbon–heteroatom coupling reactions of organometallic nickel(IV) complexes. *Science* **347**, 1218–1220 (2015).
68. Chong, E., Kampf, J. W., Ariafard, A., Canty, A. J. & Sanford, M. S. Oxidatively induced C–H activation at high valent nickel. *J. Am. Chem. Soc.* **139**, 6058–6061 (2017).
69. Omer, H. M. & Liu, P. Computational study of Ni-catalyzed C–H functionalization: factors that control the competition of oxidative addition and radical pathways. *J. Am. Chem. Soc.* **139**, 9909–9920 (2017).

Acknowledgements

This work was supported by National Natural Science Foundation of China (Nos. 22073043, 22273035), the Fundamental Research Funds for the Central Universities (No. 020514380295). We thank Dr. Liuzhou Gao, Dr. Jia Cao, and Mo Yang for their insightful discussions. All theoretical calculations were performed at the High-Performance Computing Center (HPCC) of Nanjing University.

Author contributions

X.S.S., G.Q.W., and S.H.L. conceived the work and designed the experiments. X.S.S. optimized the reaction conditions. X.S.S., L.K.H., S.D.C. and X.L.Y. performed the experiments and analyzed the experimental data. X.S.S. and G.A.L. performed the computational studies. X.S.S. and G.Q.W. co-wrote the manuscript with input from all the other authors. G.Q.W. and S.H.L. directed the project.

Competing interests

The authors declare no competing interests.

Additional information

Supplementary information The online version contains supplementary material available at https://doi.org/10.1038/s41467-024-51997-0.

Correspondence and requests for materials should be addressed to Guoqiang Wang or Shuhua Li.

Peer review information *Nature Communications* thanks the anonymous reviewer(s) for their contribution to the peer review of this work. A peer review file is available.